6-13-2014

High-Resolution Spectroscopy of the Lunar Sodium Exosphere

E. J. Mierkiewicz
Embry-Riddle Aeronautical University, mierkiee@erau.edu

R. J. Oliversen
NASA Goddard Space Flight Center

F. L. Roesler
University of Wisconsin-Madison

O. L. Lupie
NASA Goddard Space Flight Center

Scholarly Commons Citation

Mierkiewicz, E. J., R. J. Oliversen, F. L. Roesler, and O. L. Lupie (2014), High-resolution spectroscopy of the lunar sodium exosphere, J. Geophys. Res. Space Physics, 119, 4950–4956, doi:10.1002/2014JA019801

AGU PUBLICATIONS

JGR

Journal of Geophysical Research: Space Physics

RESEARCH ARTICLE

10.1002/2014JA019801

Key Point:
- Direct-line profile measurements of the lunar sodium exosphere

Correspondence to:
E. J. Mierkiewicz,
mierkiee@erau.edu

Citation:
Mierkiewicz, E. J., R. J. Oliversen, F. L. Roesler, and O. L. Lupie (2014), High-resolution spectroscopy of the lunar sodium exosphere, *J. Geophys. Res. Space Physics*, *119*, 4950–4956, doi:10.1002/2014JA019801.

Received 18 JAN 2014
Accepted 15 MAY 2014
Accepted article online 28 MAY 2014
Published online 13 JUN 2014

High-resolution spectroscopy of the lunar sodium exosphere

E. J. Mierkiewicz[1], R. J. Oliversen[2], F. L. Roesler[3], and O. L. Lupie[2]

[1]Department of Physical Sciences, Embry-Riddle Aeronautical University, Daytona Beach, Florida, USA, [2]NASA Goddard Space Flight Center, Greenbelt, Maryland, USA, [3]Department of Physics, University of Wisconsin-Madison, Madison, Wisconsin, USA

Abstract We have applied high-resolution Fabry-Perot spectroscopy to the study of the lunar sodium exosphere for the study of exospheric effective temperature and velocity variations. Observing from the National Solar Observatory McMath-Pierce Telescope, we used a dual-etalon Fabry-Perot spectrometer with a resolving power of 180,000 to measure line widths and Doppler shifts of the sodium D2 (5889.95 Å) emission line. Our field of view was 360 km, and measurements were made in equatorial and polar regions from 500 km to 3500 km off the limb. Data were obtained from full moon to 3 days following full moon (waning phase) in March 2009. Measured Doppler line widths within 1100 km of the sunlit east and south lunar limbs for observations between 5 and 40° lunar phase imply effective temperatures ranging between 3260 ± 190 and 1000 ± 135 K. Preliminary line center analysis indicates velocity displacements between different locations off the lunar limb ranging between 100 and 600 m/s from the lunar rest velocity with a precision of ±20 to ±50 m/s depending on brightness. Based on the success of these exploratory observations, an extensive program has been initiated that is expected to constrain lunar atmospheric and surface-process modeling and help quantify source and escape mechanisms.

1. Introduction

In March 2009 we conducted a successful engineering run at the McMath-Pierce (MMP) Solar Telescope using the University of Wisconsin (UW) and Goddard Space Flight Center (GSFC) Fabry-Perot Spectrometer. The goal of this run was to demonstrate the feasibility of high spectral resolution observations of sodium (Na) atoms in the lunar exosphere. Although intensities of the lunar sodium emission within a few lunar radii from the center of the Moon have been measured with good accuracy by broadband imagers [e.g., *Flynn and Mendillo*, 1993] and slit spectroscopy [e.g., *Potter and Morgan*, 1988a, 1988b; *Tyler et al.*, 1988], the velocity and temperature distribution of sodium atoms has mainly been inferred from models of observed intensity distributions [e.g., *Sprague et al.*, 2012, 1992; *Kagitani et al.*, 2010; *Potter et al.*, 2000]. An exception is a direct lunar sodium temperature measurement reported by *Stern et al.* [2000] in an abstract to the 31st Lunar and Planetary Science Conference. Based on three high-resolution spectra ($R \sim 960{,}000$) obtained on 12 September 1997, 12–24 arc sec (~20–40 km) off the east equatorial limb, *Stern et al.* [2000] derived a temperature between 1000 and 2000 K.

In this paper we report on our successful application of high-resolution Fabry-Perot spectroscopy to the study of the lunar sodium exosphere, firmly establishing a new technique for a thorough study of lunar exospheric temperature and velocity variations.

2. Instrumentation

Observations of lunar exospheric sodium line profiles requires an instrument with high signal-to-noise capability at high spectral resolution and a well-known instrumental profile in order to decompose observed profiles for hyperfine structure (roughly comparable to a 1 km/s line width), thermal widths of order 1–2 km/s, nonthermal features that may be 1–3 km/s, and nearby terrestrial sodium airglow emission. These challenges are well met by Fabry-Perot (FP) spectrometers.

The GSFC/UW FP spectrometer was originally designed for use at the North Port of the MMP to observe comet Hale-Bopp (C/1995 O1) [*Oliversen et al.*, 2002]. The FP was modified by replacing one etalon with larger spacers to increase the resolving power, and the coupling optics were replaced to match the desired etendue.

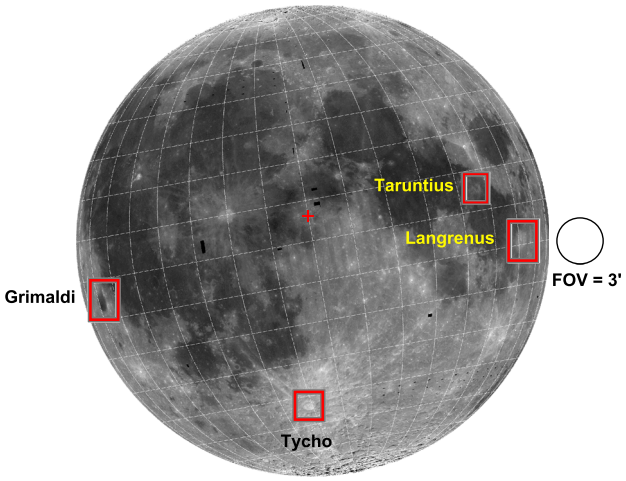

Figure 1. Observations were made in right ascension (east and west) and declination (south) out to two lunar radii above the lunar limb. Craters Grimaldi (68.3°W, 5.5°S), Taruntius (46.5°E, 5.6°N), Langrenus (61.1°E, 8.9°S), and Tycho (11.1°W, 43.4°S) were used as absolute reference points. The lunar highlands region near 0°W, 5°N was used as our "Moon center" (indicated by the cross sign in the figure). (Moon image credit: M. Robinson, Northwestern University).

The 50 mm dual-etalon FP operates in the annular summing mode [*Coakley et al.*, 1996], employing a LN2 cooled CCD camera with a 512 × 512 array of 24 μm pixels. A double-etalon FP, in which two etalons are combined in series, enables high spectral purity and contrast by extending the free spectral range Q (i.e., the spectral distance between adjacent orders of transmission) and suppressing the broad Lorentzian wings of a single etalon transmission (i.e., Airy) function [*Roesler*, 1974]. The second etalon also sharpens the common transmission peak of the two-etalon system [*Daehler and Roesler*, 1968]. The etalons are made of fused silica with highly reflective (91 ± 1% near Balmer α) broadband (~4800–9500 Å) multilayer dielectric coatings on their inward facing surfaces.

The GSFC/UW FP has a resolving etalon with a fixed gap of $l = 0.4$ cm, corresponding to a wave number free spectral range of $Q_\sigma = 1.25$ cm^{-1}. The addition of a second lower resolution etalon, with a fixed gap of $l = 0.176$ cm ($Q_\sigma = 2.84$ cm^{-1}), extends the free spectral range of the resolving etalon, by suppressing unwanted multiple orders of interference. In this configuration the instrument achieved a resolving power of ~ 180,000 (~1.7 km/s) at 5890 Å.

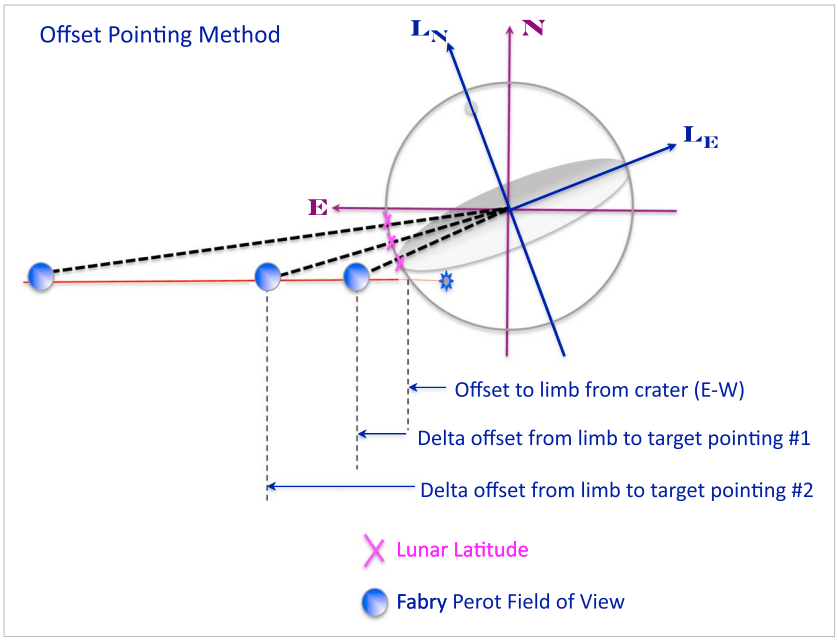

Figure 2. Observing geometry schematic using observations off crater Grimaldi (68.3°W, 5.5°S) as an example. Once centered on Grimaldi, the telescope is moved in right ascension to the limb followed by a sequence of observational steps in right ascension away from the limb. As indicated in the schematic, when moving the telescope east from Grimaldi, we are sampling the exosphere above the west limb of the Moon in selenographic coordinates. Also note that the tilt of the Moon with respect to our cardinal point observing strategy introduces a drift in lunar latitude as we scan out from the lunar limb. Latitude and altitude calculations for each observation are given in Table 1.

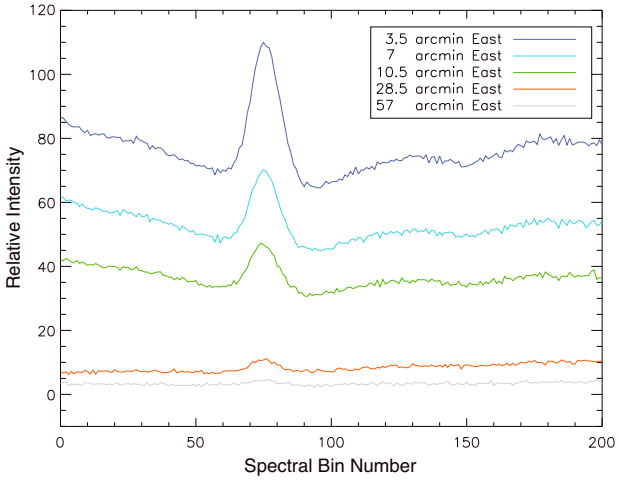

Figure 3. Lunar Na D2 emission measured at several locations off the eastern (subsolar) limb of the Moon near the Grimaldi crater (14 March 2009). Integration times were 300 s per exposure. The abscissa is in spectral bin number where 1 bin = 0.2144 km/s; red wavelengths are to the left. At a wavelength of 5890 Å the 180 bins pictured above correspond to a spectral interval of 0.76 Å (0.00421 Å per bin).

The modified FP was designed with a variable field of view (FOV), ranging from 0.5 arc min to 3 arc min, or roughly 60 km to 360 km at the Earth-Moon distance. The observations presented here were all obtained with a 3 arc min FOV, corresponding to ~360 km at the Earth-Moon distance.

3. Observations and Reduction

Observations were conducted on four successive nights (11–14) in March 2009, with most of the data taken on the nights of 13 and 14 March. Our four-night run covered a lunar phase angle of ~ 5 to 40°; observations on 11 and 12 March were taken with the Moon inside the Earth's magnetotail. We easily achieved a Na D2 signal-to-noise ratio of ~100 in 300 s at 3.5 arc min off the limb of the

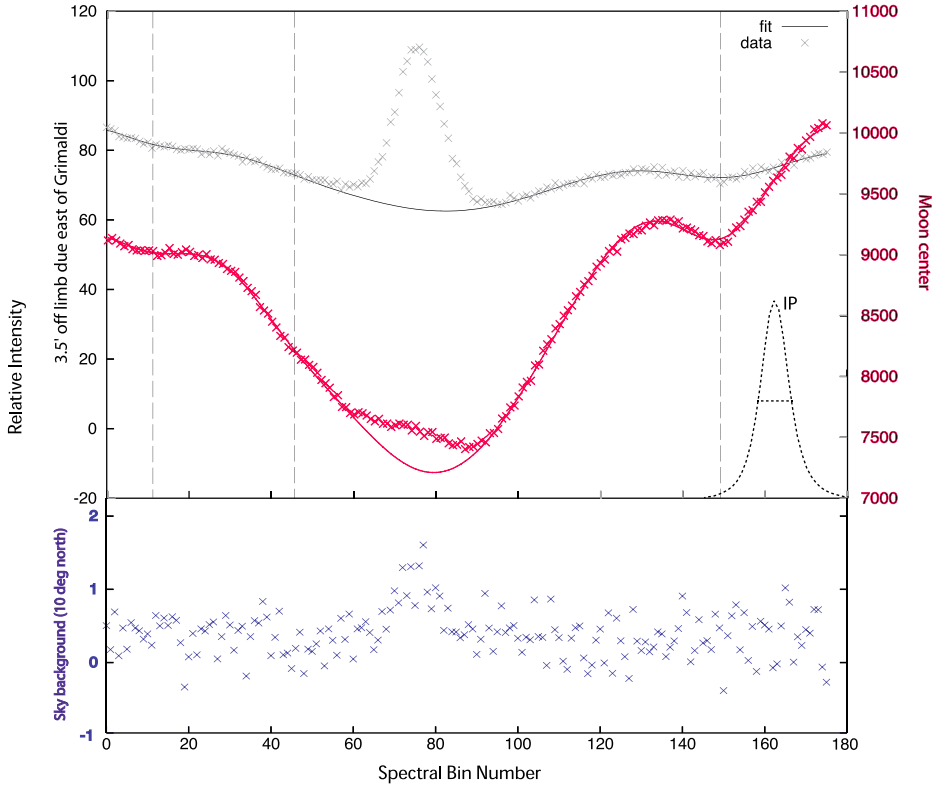

Figure 4. Sample Na spectra 3.5 arc min off the east limb (gray) and centered on the Moon (red); a sky background scan 10° north of the Moon (blue) is also included for comparison. Fits to the lunar data (solid lines) include three terrestrial H_2O lines at 5889.637, 5890.090, and 5890.227 Å (indicated by vertical dashed lines in the figure), two components for the Na emission (5889.9386 and 5889.9584 Å S-resolved hyperfine fine structure components in a 3:5 ratio), and a solar Na Fraunhofer feature at 5889.9509 Å. Note that Na emission is detected against the sunlit lunar surface (red). Integration times were 300 s for the east limb and sky background spectra; the Moon-centered spectrum was obtained in 60 s. The abscissa is in spectral bin number where 1 bin = 0.2144 km/s; red wavelengths are to the left. At a wavelength of 5890 Å the 180 bins pictured above correspond to a spectral interval of 0.76 Å (0.00421 Å per bin). A representative instrumental profile, located near spectral bin 160, is included for comparison (full width at half maximum (FWHM) ~1.7 km/s).

Table 1. Lunar Na Observations, 11–14 March 2009

Date/Time (UTC)	Phase Angle (deg)	Offset	Distance (arc min)	Distance (km)	Selenocentric Latitude (deg)	Doppler Width (km/s)	T_{eff} (K)
11 March, 05:56	4.6	Grimaldi (E)[a]	3.5	643	3.0	2.55 ± .08	3262 ± 194
11 March, 07:29	5.0	Grimaldi (E)	7	924	5.1	2.40 ± .07	2889 ± 173
11 March, 09:27	5.6	Tycho (S)[b]	3.5	730	−70.9	2.21 ± .06	2458 ± 127
11 March, 09:40	5.7	Tycho (S)	3.5	730	−70.9	2.20 ± .07	2430 ± 144
12 March, 09:36	17.3	Grimaldi (E)	3.5	612	2.2	1.95 ± .08	1908 ± 144
12 March, 09:48	17.3	Grimaldi (E)	7	943	4.9	1.99 ± .08	1992 ± 159
13 March, 09:14	29.5	Grimaldi (E)	3.5	575	1.1	1.72 ± .04	1474 ± 69
13 March, 09:23	29.5	Grimaldi (E)	7	929	2.6	1.63 ± .07	1330 ± 116
13 March, 09:32	29.6	Grimaldi (E)	10.5	1288	6.2	1.72 ± .10	1474 ± 165
13 March, 09:42	29.6	Grimaldi (E)	14	1651	7.9	1.69 ± .10	1438 ± 163
13 March, 09:51	29.7	Grimaldi (E)	30	3332	12.6	1.65 ± .14	1366 ± 214
13 March, 10:45	29.9	Langrenus (W)[c]	3.5	818	−18.3	2.25 ± .17	2540 ± 363
13 March, 10:53	30.0	Langrenus (W)	7	1193	−18.8	2.19 ± .15	2397 ± 326
13 March, 11:03	30.0	Langrenus (W)	10.5	1568	−19.1	2.40 ± .28	2889 ± 632
13 March, 11:11	30.1	Langrenus (W)	14	1943	−19.4	1.89 ± .34	1784 ± 590
13 March, 11:20	30.1	Langrenus (W)	17.5	2319	−19.7	1.84 ± .28	1704 ± 476
13 March, 11:30	30.2	Langrenus (W)	30	3661	−20.3	1.87 ± .21	1744 ± 378
14 March, 07:05	40.8	Grimaldi (E)	3.5	554	0.0	1.59 ± .04	1261 ± 64
14 March, 07:16	40.8	Grimaldi (E)	7	894	2.7	1.59 ± .07	1261 ± 110
14 March, 07:25	40.9	Grimaldi (E)	10.5	1265	4.9	1.61 ± .08	1296 ± 118
14 March, 07:35	41.0	Grimaldi (E)	28.5	3140	10.7	1.24 ± .17	775 ± 199
14 March, 08:22	41.2	Tycho (S)	3.5	796	−72.1	1.61 ± .05	1296 ± 78
14 March, 08:32	41.3	Tycho (S)	7	1137	−72.8	1.42 ± .10	1003 ± 135
14 March, 08:42	41.3	Tycho (S)	10.5	1553	−72.4	1.59 ± .13	1261 ± 193
14 March, 08:52	41.4	Tycho (S)	30	3735	−71.2	1.22 ± .18	748 ± 200
14 March, 09:35	41.6	Taruntius (W)[d]	4	736	−10.8	2.34 ± .20	2737 ± 452
14 March, 09:46	41.7	Taruntius (W)	10.5	1418	−12.8	1.97 ± .17	1950 ± 324

[a]Off lunar limb east of Grimaldi.
[b]Off lunar limb south of Tycho.
[c]Off terminator west of Langrenus.
[d]Off terminator west of Taruntius.

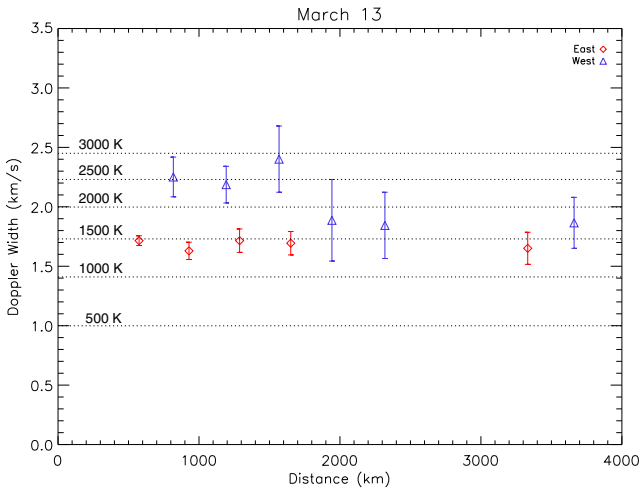

Figure 5. On 13 March 2009, Doppler width as a function of distance off the limb of the Moon (lunar phase angle ~30°). Observations off the west terminator intersect the Moon's shadow; Doppler widths measured in the west below 1800 km are broader than their counterparts in the east. Horizontal lines of constant temperature in steps of 500 K are included for comparison.

Moon with our 3 arc min FOV. Sodium emission was measured in three cardinal directions (south, east, and west) out to two lunar radii above the lunar limb.

Our observing strategy was to center on one of four identifiable craters: Grimaldi, Tycho, Langrenus, and Taruntius; refer to Figure 1. Once centered, we moved the telescope in right ascension or declination to the limb and then moved the telescope in observational steps (right ascension or declination) away from the limb; refer to Figure 2. All observations were collected with the telescope tracking at the lunar rate; tracking errors relative to the Moon were on the order of 15 arc sec over a 5 min integration. The telescope was recentered on the relevant crater before each step. Examples of the data obtained off the eastern (subsolar) limb in steps of right ascension are given in Figure 3.

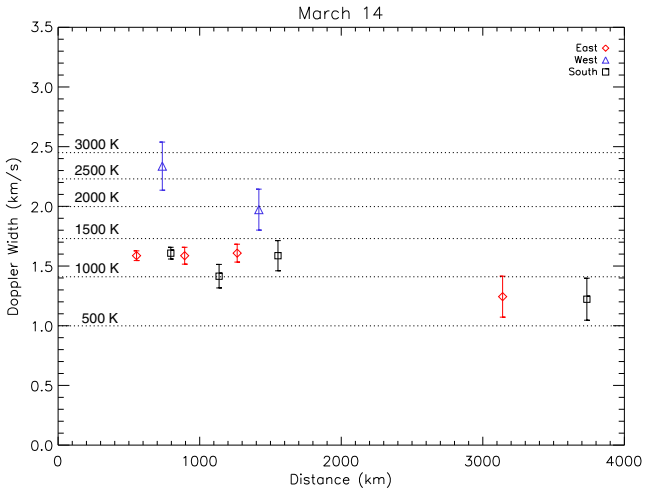

Figure 6. On 14 March 2009, Doppler width as a function of distance off the limb of the Moon (lunar phase angle ~41°). Observations off the west terminator intersect the Moon's shadow; Doppler widths measured in the west below 1800 km are broader than their counterparts in the east and south. Horizontal lines of constant temperature in steps of 500 K are included for comparison.

Individual lunar spectra were reduced with a six-component Gaussian model convolved with a measured instrumental function. The model was fit to the spectrum using the least squares fitting code of R. C. Woodward (A parameter estimation technique for spectral analysis of overlapping lines, private communication, 2014). The instrumental function and wavelength calibration were determined using a Thorium I line at 5891.451 Å. Two emission components were used to fit the lunar sodium emission accounting for Na D2 S-resolved hyperfine structure with components at 5889.9386 and 5889.9584 Å in a 3:5 emission ratio [*McNutt and Mack*, 1963]. A single component was used to fit the broad solar Fraunhofer D2 absorption. Three additional components were used to fit terrestrial H_2O absorption lines at 5889.637, 5890.090, and 5890.227 Å. Refer to Figure 4. Note that the Fraunhofer line does not go to 5% of the continuum due to parasitic light contamination from a continuum source. A much smaller contribution is due to Brillouin scattering [*Potter et al.*, 1984] filling in the Fraunhofer line.

Terrestrial sodium emission contamination was minor. Background measurements (see Figure 4) taken 10° away from the Moon indicate lunar sodium measurements one lunar radius off the limb have less than about a 15% contribution due to terrestrial sodium emission.

Wavelength and instrument profile calibrations were determined by monitoring the Thorium I line, 5891.451 Å. Thorium line center measurements on 13 and 14 March indicated small shifts due to temperature changes in the observing room with a shift of <0.1 spectral bins per hour (1 bin = 0.2144 km/s).

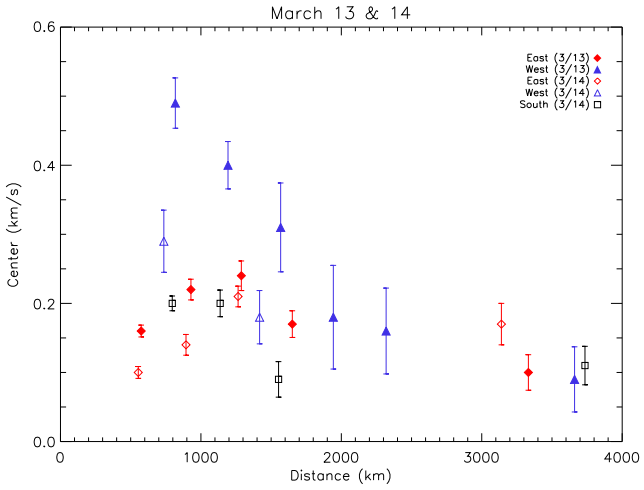

Figure 7. On 13 and 14 March 2009, line center position as a function of distance off the limb of the Moon. The velocities are in the lunar frame of reference, corrected for the Earth-Moon topocentric velocities and small time-dependent instrument drift. Note that observations off the west terminator intersect the Moon's shadow; here we observe our highest shifts in line center position.

A spectral scale in units of velocity (km/s) is used in this paper, where $\Delta\lambda/\lambda_o = v/c$. Doppler line widths will also be reported in terms of effective temperatures T_{eff}, where

$$T_{\text{eff}} = 4.51 \times 10^{13} \left(\frac{\Delta\lambda_{\text{FWHM}}}{\lambda_o} \right)^2 \text{[K]}. \quad (1)$$

4. Results

Observation parameters (lunar phase angles, distances, and selenocentric latitudes), Doppler widths, and effective temperatures are listed in Table 1. Measured Doppler line widths within 1100 km of the east and south lunar limbs for observations between 5 and 40° lunar phase imply temperatures ranging between 3260 ± 190 and 1000 ± 135 K. For nights with the best coverage (13 and 14 March) we measure effective temperatures of ~1430 K (13 March) and ~1230 K (14 March)

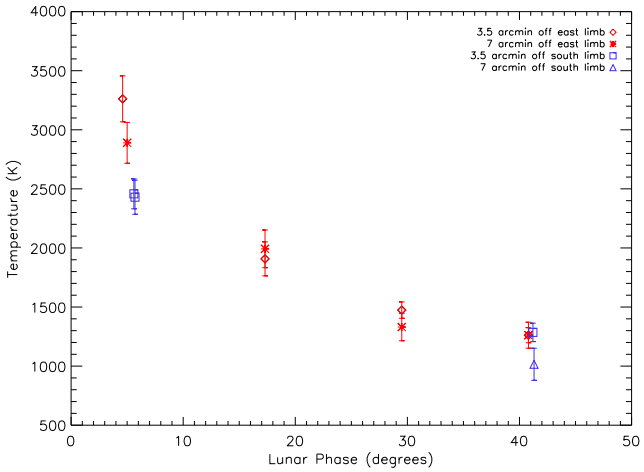

Figure 8. The Doppler line width as a function of lunar phase with observations taken at 3.5 and 7 arc min (<1100 km) off the eastern and southern limbs from successive nights during 11–14 March 2009. Measured Doppler line widths imply temperatures ranging between 3260 ± 190 and 1000 ± 135 K.

within 1800 km of the east and south lunar limbs. Observations off the west terminator on 13–14 March intersect the Moon's shadow (lunar waning phase); Doppler widths measured in the west below 1800 km are broader than their counterparts in the east and south. Refer to Figures 5 and 6.

In line center analysis we also note velocity displacements between the west, east, and south lunar limbs, ranging between 100 and 600 m/s from the lunar rest velocity; our line center precision is ±20 to ±50 m/s depending on brightness. Refer to Figure 7.

5. Discussion

Observations taken 3.5 and 7 arc min off the east and south limbs (11–14 March) indicate a change in Doppler width correlated with lunar phase. In terms of effective temperature, we observed a decrease from 3260 ± 190 K near full moon to 1000 ± 135 K at a phase angle of 42°; refer to Figure 8.

A similar result was reported by *Potter et al.* [2000] in their interpretation of the observed altitude dependence of sodium emission intensity with lunar phase. In analysis of sodium scale heights derived from their emission measurements, *Potter et al.* [2000] found scale heights to be largest near full moon, decreasing with increasing lunar phase angle. This change in scale height with phase translates into a decrease in derived exospheric temperatures, from 2900 K (4.3° phase angle) to 1200 K (33.7° phase angle) with the decrease occurring more rapidly during the waxing phase. Our 11–14 March *waning* phase observations are in close agreement with the *Potter et al.* [2000] *waxing* phase observations; refer to Figure 9.

Potter et al. [2000] point out that their observed phase dependence on scale height derived temperatures may be an apparent effect, the result of the geometry of the lunar sodium exosphere. Near full moon the observed line of sight looks down the lunar tail, invalidating the assumption of a spherically symmetric exosphere and perhaps leading to higher derived temperatures. This signature should manifest itself as an extended red wing in our line profile observations at full moon. We have not detected a phase-dependent red-wing asymmetry.

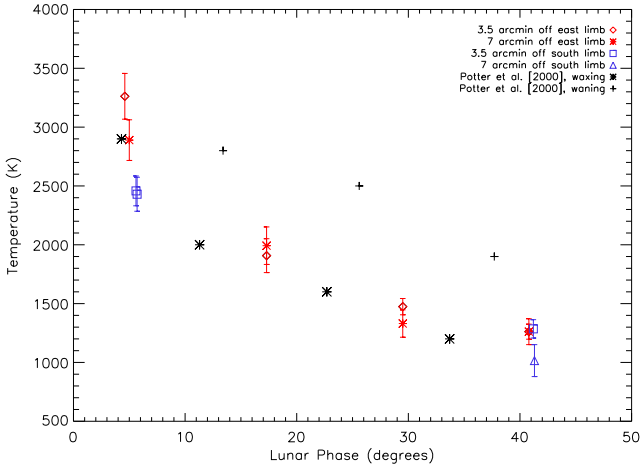

Figure 9. Comparison of our direct temperature observations and those determined by *Potter et al.* [2000]. Note that although our observations were obtained during the waning phase, we find better agreement with the waxing phase derived temperatures of *Potter et al.* [2000].

Similar to the scale height derived temperatures of *Potter et al.* [2000], *Sprague et al.* [2012, 1992], and other observers (see the review by *Stern* [1999]), our measured effective temperatures are larger than expected for sodium atoms thermalized to the surface temperature of ~400 K, indicating that the source of these exospheric particles is, at least in part, an energetic nonthermal process such as photon-stimulated desorption [see, e.g., *Madey et al.*, 1998; *Sarantos et al.*, 2010]. Future velocity-resolved line profile observations under different lunar phases including in and out of the Earth's

magnetotail and measurements at different altitudes and latitudes will be used to explore factors that link observed morphologies and dynamics to the sources, sinks, and escape of the lunar atmosphere. These observations will help constrain atmospheric and surface-process modeling and help quantify source and escape mechanisms.

Acknowledgments

The authors thank the National Solar Observatory and the Kitt Peak mountain staff for their efforts in making this engineering run so successful. We also thank K. Jaehnig for his invaluable engineering support and undergraduate students S.A. Sans, NASA summer internship program, and S.C. McKillop for their participation in data analysis. This work was supported by NASA Planetary Astronomy award NNX11AE38G and NNX13AL30G.

Alan Rodger thanks the reviewers for their assistance in evaluating this paper.

References

Coakley, M. M., F. L. Roesler, R. J. Reynolds, and S. Nossal (1996), Fabry-Perot CCD annular-summing spectroscopy: Study and implementation for aeronomy, *Appl. Opt.*, *35*, 6479–6493.

Daehler, M., and F. L. Roesler (1968), High contrast in a polyetalon Fabry-Perot spectrometer, *Appl. Opt.*, *7*, 1240–1241.

Flynn, B., and M. Mendillo (1993), A picture of the Moon's atmosphere, *Science*, *261*, 184–186.

Kagitani, M., M. Taguchi, A. Yamazaki, I. Yoshikawa, G. Murakami, K. Yoshioka, S. Kameda, and S. Okano (2010), Variation in lunar sodium exosphere measured from lunar orbiter SELENE (Kaguya), *Planet. Space Sci.*, *58*(12), 1660–1664.

Madey, T. E., B. V. Yakshinskiy, V. N. Ageev, and R. E. Johnson (1998), Desorption of alkali atoms and ions from oxide surfaces—Relevance to origins of NA and K in atmospheres of Mercury and the Moon, *J. Geophys. Res.*, *103*, 5873–5887.

McNutt, D. P., and J. E. Mack (1963), Telluric absorption, residual intensities, and shifts in the Fraunhofer D lines, *J. Geophys. Res.*, *68*, 3419–3429.

Oliversen, R. J., N. Doane, F. Scherb, W. M. Harris, and J. P. Morgenthaler (2002), Measurements of [CI] emission from comet Hale-Bopp, *Astrophys. J.*, *581*, 770–775.

Potter, A. E., W. Mendell, and T. H. Morgan (1984), Lunar luminescence and the filling-in of the Fraunhofer lines in moonlight, *J. Geophys. Res.*, *89*(S01), C240–C244.

Potter, A. E., and T. H. Morgan (1988a), Discovery of sodium and potassium vapor in the atmosphere of the Moon, *Science*, *241*, 675–680.

Potter, A. E., and T. H. Morgan (1988b), Extended sodium exosphere of the Moon, *Geophys. Res. Lett.*, *15*, 1515–1518.

Potter, A. E., R. M. Killen, and T. H. Morgan (2000), Variation of lunar sodium during passage of the Moon through the Earth's magnetotail, *J. Geophys. Res.*, *105*, 15,073–15,084.

Roesler, F. L. (1974), Fabry-Perot instruments for astronomy, in *Methods of Experimental Physics, Part A: Optical and Infrared*, vol. 12, edited by M. Carlton, 531 pp., Academic Press, New York.

Sarantos, M., R. M. Killen, S. A. Surjalal, and J. A. Slavin (2010), Sources of sodium in the lunar exosphere: Modeling using ground-based observations of sodium emission and spacecraft data of the plasma, *Icarus*, *205*, 364–374.

Sprague, A. L., R. W. H. Kozlowski, D. M. Hunten, W. K. Wells, and F. A. Grosse (1992), The sodium and potassium atmosphere of the Moon and its interaction with the surface, *Icarus*, *96*, 27–42.

Sprague, A. L., M. Sarantos, D. M. Hunten, R. E. Hill, and R. W. H. Kozlowski (2012), The lunar sodium atmosphere: April–May 1998, *Can. J. Phys.*, *90*, 725–732.

Stern, S. A. (1999), The lunar atmosphere: History, status, current problems, and context, *Rev. Geophys.*, *37*, 453–492.

Stern, S. A., A. Fitzsimmons, R. M. Killen, and A. E. Potter (2000), A direct measurement of sodium temperature in the lunar atmosphere, *31st Annual Lunar and Planetary Science Conference,* March 13–17, 2000, Houston, Texas, Abstract 1122.

Tyler, A. L., D. M. Hunten, and R. Kozlowski (1988), Observations of sodium in the tenuous lunar atmosphere, *Geophys. Res. Lett.*, *15*, 1141–1144.